The Astrophysical Journal, 860:56 (5pp), 2018 June 10 https://doi.org/10.3847/1538-4357/aac2d3

Dynamical Constraints on the Dark Matter Distribution of the Sculptor Dwarf Spheroidal from Stellar Proper Motions

Louis E. Strigari[1], Carlos S. Frenk[2], and Simon D. M. White[3]
[1] Mitchell Institute for Fundamental Physics and Astronomy, Department of Physics and Astronomy, Texas A & M University, College Station, TX 77843, USA
[2] Institute for Computational Cosmology, Department of Physics, University of Durham, South Road, Durham DH1 3LE, UK
[3] Max-Planck-Institut für Astrophysik, Karl-Schwarzschild-Straße 1, D-85740 Garching bei München, Germany
Received 2018 February 7; revised 2018 April 11; accepted 2018 May 3; published 2018 June 12

Abstract

We compare the transverse velocity dispersions recently measured within the Sculptor dwarf spheroidal galaxy to the predictions of our previously published dynamical model. This was designed to fit the observed number count and velocity dispersion profiles of both metal-rich and metal-poor stars, both in cored and in cusped potentials. At the projected radius where the proper motions (PMs) were measured, this model (with no change in parameters) predicts transverse dispersions in the range of 6–9.5 km s^{-1}, with the tangential dispersion about 1 km s^{-1} larger than the (projected) radial dispersion. Both dispersions are predicted to be about 1 km s^{-1} larger for metal-poor than for metal-rich stars. At this projected radius, cored and cusped potentials predict almost identical transverse dispersions. The measured tangential dispersion (8.5 ± 3.2 km s^{-1}) agrees remarkably well with these predictions, while the measured radial dispersion (11.5 ± 4.3 km s^{-1}) differs only at about the 1σ level. Thus, the PM data are in excellent agreement with previous data, but do not help to distinguish between cored and cusped potentials. This will require velocity dispersion data (either from PMs or from radial velocities) with uncertainties well below 1 km s^{-1} over a range of projected radii.

Key words: dark matter – galaxies: dwarf – Local Group

1. Introduction

The kinematics of stars in the central regions of dark matter-dominated dwarf spheroidal galaxies (dSphs) may allow us to distinguish between different hypotheses for the nature of dark matter. On these scales the simplest "Lambda cold dark matter" (ΛCDM) model of structure formation predicts cuspy halos that are well described by the Navarro–Frenk–White (NFW) profile (Navarro et al. 1996, 1997, 2010). Alternative forms of dark matter, such as self-interacting (Spergel & Steinhardt 2000; Vogelsberger et al. 2012; Rocha et al. 2013) or warm (Bode et al. 2001; Lovell et al. 2016) dark matter predict low-mass halos with either a constant density core or a shallower central cusp.

Published analyses of the line-of-sight (LOS) velocities of stars in dSphs have led to contradictory conclusions: some authors conclude that the kinematic data require dark matter cores (Gilmore et al. 2007; Walker & Penarrubia 2011; Agnello & Evans 2012), while others find that the data are also consistent with NFW-like cusps (Strigari et al. 2010, 2017; Breddels et al. 2013; Richardson & Fairbairn 2014).

Accurate measurements of stellar proper motions (PMs) can further constrain the central density in dSphs (Wilkinson et al. 2002; Strigari et al. 2007; Read & Steger 2017). Together with LOS velocities and positions on the sky, the two additional transverse velocity components provide five out of the six phase space coordinates of the stars. These data can help break the degeneracy between stellar velocity anisotropy and the galaxy mass profile, which has so far been a limiting factor in kinematical studies of dSphs. Since thousands of LOS velocities are already available for the best studied cases, such as Fornax and Sculptor (Walker et al. 2009), precise measurements of the transverse velocity dispersions are required to improve constraints on the inner dark matter density profile.

In a recent landmark study Massari et al. (2017) have measured sufficiently accurate PMs for a number of stars in Sculptor for the uncertainty in their transverse velocity dispersion estimates to be significantly smaller than the intrinsic velocity dispersion of the system. This is the first time such a measurement has been performed in a dSph with this level of accuracy, thus finally opening the era of using dynamical models with full phase space information to constrain the inner dark matter distribution of dSphs.

Here, we use the self-consistent stellar distribution function model for Sculptor published by Strigari et al. (2017) to predict transverse velocity dispersions at the position where these were measured by Massari et al. (2017). Sculptor has two distinct metallicity populations (Battaglia et al. 2008; Walker et al. 2009). The Strigari et al. (2017) models treat the metal-rich (MR) and metal-poor (MP) components as separate populations orbiting in a common gravitational potential which may be cusped or cored. They were fit directly to the position and LOS velocity data of Walker et al. (2009). As we will see, the same model, with no change in parameter values, predicts transverse dispersions in good agreement with the new measurements by Massari et al. (2017) in both cases. At the end of our paper we discuss the accuracy of PM and LOS velocity dispersion measurements that will be required robustly to distinguish a core from a cusp in the dark matter distribution of this galaxy.

The Strigari et al. (2017) model that we use here assumes that each metallicity population is spherically symmetric and in dynamical equilibrium within a static and spherically symmetric potential. These are strong assumptions that should be kept in mind. The observed stellar distribution in Sculptor is clearly elongated on the sky and the galaxy is moving on a non-circular orbit around the Milky Way, thus experiencing a time-varying tidal potential. Some of the effects of a flattened internal potential on the observable velocity dispersions are

discussed by Agnello & Evans (2012) and Laporte et al. (2013).

2. Data

To measure the PMs of stars in Sculptor, Massari et al. (2017) combined astrometry from the first *Gaia* data release with positions from two overlapping *Hubble Space Telescope* (*HST*) fields, which have an average projected radius of $R = 185$ pc from the center of Sculptor. With an approximate 12 year baseline between the observations, 15 stars with particularly well-measured PMs allowed them to estimate the transverse radial and tangential velocity dispersions at this position in Sculptor as $\sigma_R(R = 185\,\mathrm{pc}) = 11.5 \pm 4.3\,\mathrm{km\,s^{-1}}$ and $\sigma_T(R = 185\,\mathrm{pc}) = 8.5 \pm 3.2\,\mathrm{km\,s^{-1}}$, respectively.

The combination of these new transverse dispersion estimates with earlier estimates of the LOS velocity dispersion profile of Sculptor based on large numbers of stars (Battaglia et al. 2008; Walker et al. 2009) provides the highest quality kinematic data set ever assembled for a dSph. There is some ambiguity in how best to identify the stars that belong to the MR and MP populations and thus, to estimate the velocity dispersion and star count profiles for each population (Battaglia et al. 2008; Walker & Penarrubia 2011; Amorisco & Evans 2012; Strigari et al. 2017). Here we split the data of Walker et al. (2009) into distinct populations as described in Strigari et al. (2017); this results in a sample of 397 MR and 763 MP stars.

3. Models and Data Analysis

We now briefly describe the dynamical model that we use to analyze the Sculptor data and our statistical method for predicting the transverse velocity dispersion from the Walker et al. (2009) data.

For the dark matter profile we consider two well-studied models, one characterized by a central cusp and the other by a central core. For the cusped model, we adopt the NFW profile (Navarro et al. 1996, 1995),

$$\rho(r) = \frac{\rho_s}{x(1+x)^2}, \tag{1}$$

where ρ_s is the scale density and $x = r/r_s$ with r_s as the scale radius. For the cored model we adopt the Burkert profile (Burkert 1995),

$$\rho(r) = \frac{\rho_b}{(1+x_b)(1+x_b^2)}, \tag{2}$$

where ρ_b is the Burkert scale density and $x_b = r/r_b$ with r_b as the Burkert scale radius.

For the stellar distribution function we adopt the model of Strigari et al. (2017). Here we briefly review the relevant aspects of this model and refer to this paper and to White (1981) for a more detailed discussion. The specific energy and specific angular momentum of a star are $E = v^2/2 + \Phi(r)$ and $J = vr\sin\theta$, respectively, where v is the modulus of the velocity vector, $\Phi(r)$ is the gravitational potential derived from the density profile (assuming spherical symmetry), and θ is the angle between this vector and the star's position vector relative to the center of the system. If we assume that the dependence on E and J is separable, we then have

$$f(E, J) = g(J)h(E), \tag{3}$$

where both $g(J)$ and $h(E)$ are positive definite and have the simple parametric forms as discussed below.

The stellar density profile and the radial and tangential velocity dispersion profiles are given by

$$\rho_\star(r) = 2\pi \int_0^\pi d\theta \sin\theta \int_0^{v_{\rm esc}} dv v^2 g(J) h(E), \tag{4}$$

$$\rho_\star \sigma_r^2(r) = 2\pi \int_0^\pi d\theta \cos^2\theta \sin\theta \int_0^{v_{\rm esc}} dv v^4 g(J) h(E), \tag{5}$$

$$\rho_\star \sigma_t^2(r) = \pi \int_0^\pi d\theta \sin^2\theta \sin\theta \int_0^{v_{\rm esc}} dv v^4 g(J) h(E), \tag{6}$$

where $v_{\rm esc} = \sqrt{2[\Phi_{\rm lim} - \Phi(r)]}$, with $\Phi_{\rm lim}$ defined as the value of the potential at the limiting radius. The total velocity dispersion at radius r is then

$$\sigma_{\rm tot}^2(r) = \sigma_r^2(r) + 2\sigma_t^2(r). \tag{7}$$

Equations (4)–(6) can be combined to give the projected stellar density profile and the stellar LOS and transverse velocity dispersion profiles at a fixed projected distance, R,

$$I_\star(R) = 2\int_0^\infty \rho_\star(r) dz, \tag{8}$$

$$I_\star(R)\sigma_{\rm los}^2(R) = 2\int_0^\infty \rho_\star(r) \frac{z^2\sigma_r^2 + R^2\sigma_t^2}{z^2 + R^2} dz, \tag{9}$$

$$I_\star(R)\sigma_R^2(R) = 2\int_0^\infty \rho_\star(r) \frac{R^2\sigma_r^2 + z^2\sigma_t^2}{z^2 + R^2} dz, \tag{10}$$

$$I_\star(R)\sigma_T^2(R) = 2\int_0^\infty \rho_\star(r)\sigma_t^2 dz, \tag{11}$$

where $r^2 = z^2 + R^2$. Here R is the radial component in the plane of the sky, pointing radially outward from the center of the galaxy. The component T is tangential to R, and is also in the plane of the sky.

In the model of Strigari et al. (2017) the energy part, $h(E)$, is a function of seven parameters; the angular momentum component, $g(J)$, is a function of four parameters; and the density profiles in Equations (1) and (2) are functions of two parameters. Thus, for a single stellar population the model has 13 parameters. When performing a joint fit to both metallicity populations, in which each population has independent distribution function parameters but the common underlying dark matter profile is still a function of two parameters, the model has a total of 24 free parameters. In Strigari et al. (2017) we used a slightly simpler model in which the velocity distribution is assumed to be isotropic near the center. This model has a total of 20 parameters and is the one we use in this paper; the parameter values are listed in Table 1 of Strigari et al. (2017).

To fit this distribution function to the LOS velocities and the photometry of Walker et al. (2009) for each population, we define a likelihood function as in Strigari et al. (2017). From this likelihood function we employ a Nested Sampling algorithm to scan over the parameter space (Handley et al. 2015a, 2015b) and determine the posterior probability density for the model parameters. The Nested Sampling algorithm is particularly useful for sampling the posteriors of high dimensional parameter spaces which may contain multiple regions of high probability. In our code we use 500 live points and obtain the posterior probability densities for the model parameters, as well as for the parameters that are derived from

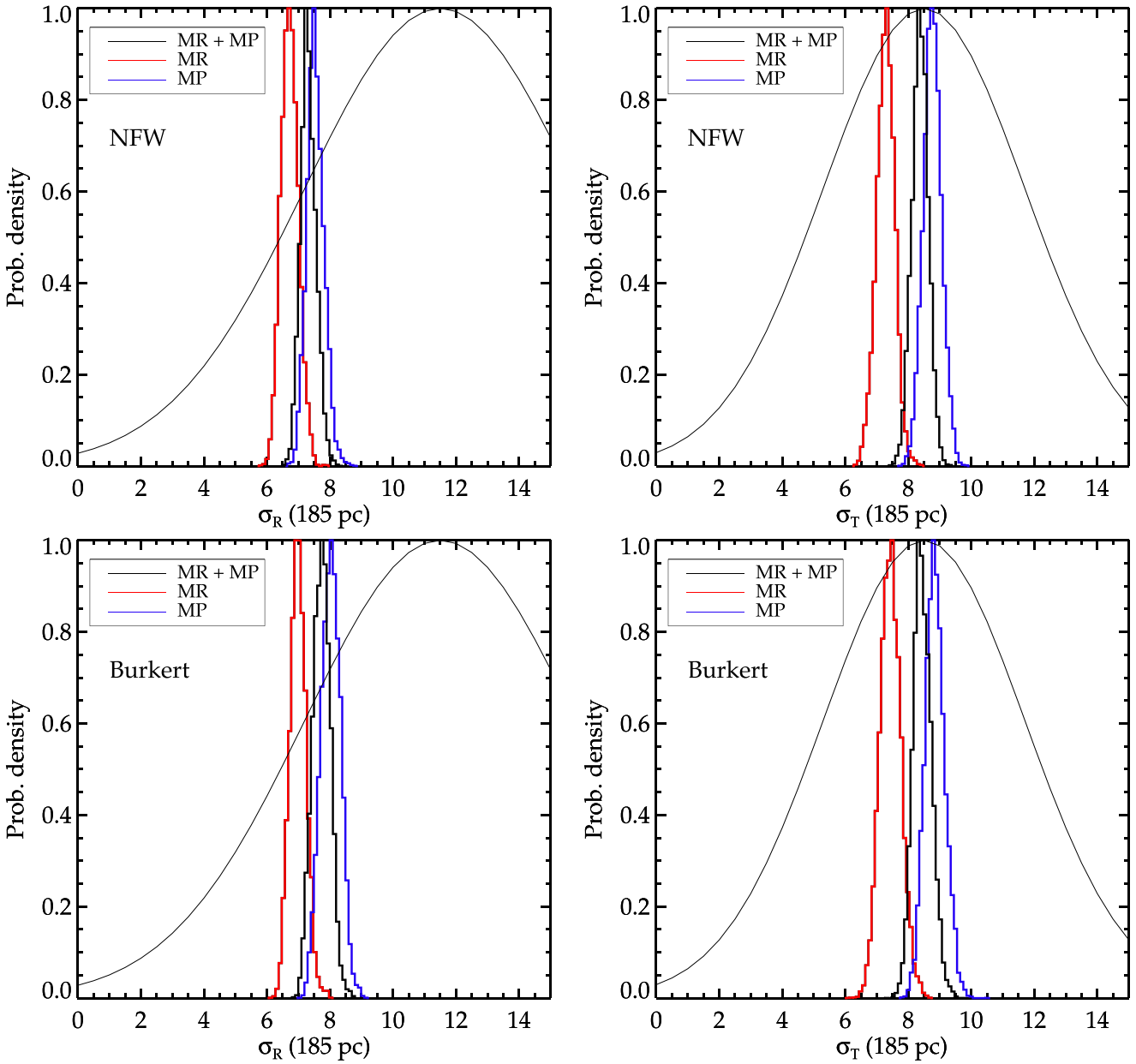

Figure 1. Posterior probability densities for the transverse radial and tangential velocity dispersions for different populations, based on the models of Strigari et al. (2017) which fit parameterized distribution functions to star count and LOS velocity dispersion data from Walker & Penarrubia (2011). The top row assumes an NFW dark matter profile and the bottom row a Burkert profile. The red histogram is for the MR population, the blue histogram is for the MP population, and the black histogram for the total population. The thin black curves are Gaussian distributions that represent the PM-based estimates of Massari et al. (2017) and their 1σ uncertainty.

them. While there are degeneracies in the model parameters that describe the stellar distribution function, the projected transverse velocity dispersions, σ_R and σ_T, which are derived from the models, are well determined in all cases.

4. Results

We now present predictions for the transverse velocity dispersions at the position of the Massari et al. (2017) measurements based on a joint analysis of the LOS velocity dispersion and photometric count profiles for the MR and MP populations. The posterior probability distributions for these transverse velocity dispersions are shown in Figure 1 for three different populations: the MP population, the MR population, and the total population. For this third case, the total dispersion at projected radius, R, is

$$\sigma^2(R) = f_{\rm MR}(R)\sigma^2_{\rm MR}(R) + [1 - f_{\rm MR}(R)]\sigma^2_{\rm MP}(R), \qquad (12)$$

where $f_{\rm MR}(R)$ is defined as the fraction of MR stars at projected radius, R. We evaluate $f_{\rm MR}(R = 185\,{\rm pc})$ for each photometric model, with the profiles normalized by the number of stars in each population, accounting for the selection function from Walker & Penarrubia (2011). The fraction of MR stars is then given by

$$f_{\rm MR}(R) = \frac{I_{\rm MR}(R)}{I_{\rm MR}(R) + I_{\rm MP}(R)}, \qquad (13)$$

where the I's are the normalized photometric profiles.

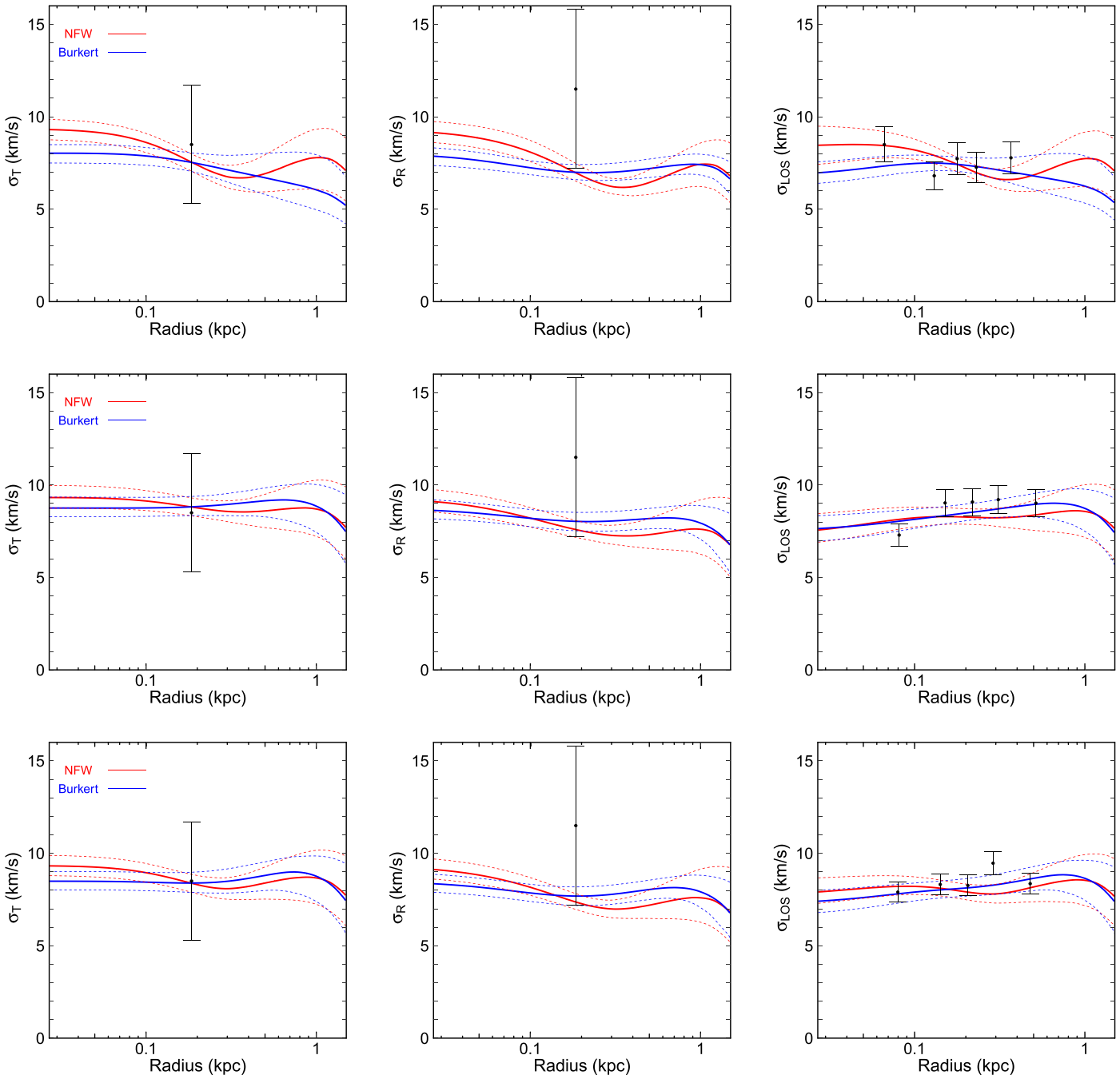

Figure 2. Predicted velocity dispersions for the MR (top), MP (middle), and combined populations. In each panel, the red is for the NFW profile and the blue for the Burkert profile. The solid curves are the mean of the posterior distribution at each radius and the dashed curves encompass its 10%–90% range. The symbols with error bars show the values of the transverse tangential and radial dispersions derived from the PM measurements by Massari et al. (2017) and the LOS dispersion of each population estimated by Strigari et al. (2017) based on data from Walker & Penarrubia (2011).

Figure 1 shows that there is excellent agreement between the value of σ_T predicted by our model based on the Walker et al. (2009) data and that measured from the PMs. For σ_R, the model prediction differs from the measurement at the $\sim 1\sigma$ level. This is true for both NFW and Burkert profiles. The model prediction agrees slightly better with the measurement if we assume that the stars with measured PMs are randomly drawn from the MP population or from the entire population (as expressed in Equation (12)) than if we assume they are drawn from the MR population. However, Massari et al. (2017) suggest, based on estimates of metallicity, that their PM sample may be dominated by MR stars.

While the current PM data are unable to distinguish between the NFW and the Burkert density profiles, it is interesting to ask whether this will be possible with a larger sample of PM measurements. A rough answer to this question is given by Figure 2 where we plot the range of transverse radial, transverse tangential, and LOS velocity dispersion profiles that are compatible with the observed LOS velocity dispersion and number count data according to our model. At each projected radius, we calculate the posterior distribution of each of the three velocity dispersion components from our Monte Carlo sampling. We show its mean as a solid curve and enclose its 10%–90% range with dashed curves. The points with error bars

in the left and middle panels are the PM-based measurements of Massari et al. (2017), while for the LOS velocity dispersion we plot the binned estimates of Strigari et al. (2017) for the MR, MP, and total MR+MP populations. These are based on the observational data of Walker & Penarrubia (2011).

The largest difference between the predictions for the NFW and Burkert dark matter profiles occurs at radii less than the approximate half-light radius and is most apparent in the MR population. Even in this case, however, the differences between the two models are less than 2 km s^{-1}. Interestingly, the LOS data alone have very similar discriminating power as the projected radial and tangential dispersions. Taking a simple estimate of the sampling error on each velocity dispersion as $\sim\sigma_R/\sqrt{2N}$, our results imply that distinguishing between the NFW and Burkert profiles at the $\sim 2\sigma$ level will require measurements of PMs or LOS velocities for a few thousand stars with individual uncertainties well below 5 km s^{-1} and spread evenly over the radial range of $1.5 < \log_{10}(R/1\ \mathrm{pc}) < 2.7$.

5. Discussion and Conclusion

We have performed a dynamical analysis of internal stellar PMs in the Sculptor dSph. Using our earlier dynamical model (Strigari et al. 2017), we compared the predicted tangential velocity dispersions derived from LOS velocity dispersion and star count data to direct estimates derived from the recently measured PMs of 15 stars by Massari et al. (2017). We have shown that there is excellent consistency between the predicted and directly measured projected tangential velocity dispersion, while the predicted and directly measured projected radial velocity dispersions differ only at $\sim 1\sigma$.

The agreement between the model predictions and the data is just as good for models that assume an NFW profile for the dark matter as for models that assume a Burkert profile. Thus, even with the new PM data we are unable to resolve the long-standing "core/cusp" controversy over the dark matter distribution in the center of Sculptor. The observational uncertainties in the count and velocity dispersion profiles are still large enough to mask the difference between the two potentials even with observational information on five out the six phase space coordinates. However, we have shown that, in principle, the controversy can be resolved with larger samples of precise velocities, either LOS or from PMs, provided a substantial fraction of the measurements are at small projected radii. We have checked that splitting the stars into distinct metallicity populations with different radial distributions enhances the accuracy with which our distribution function-based dynamical model can constrain the potential. Thus, obtaining good quality spectra to allow metallicity determinations is also important. Finally, improved photometry to reduce uncertainties in the projected stellar count profiles would also be helpful.

The pioneering work of Massari et al. (2017) has demonstrated that internal PM measurements for stars in dSphs can be made with sufficiently small errors to allow interesting dynamical modeling. Upcoming *Gaia* data releases will lead to a dramatic improvement in the amount and quality of PM data for bright dSphs. Together with new ground-based photometric and spectroscopic campaigns on these objects, this offers the exciting prospect of finally allowing robust inferences about the central dark matter distribution in these galaxies and thus about the nature of dark matter.

L.E.S. is supported by the U.S. Department of Energy award de-sc0010813. This work was also supported by the Science and Technology Facilities Council grants ST/L00075X/1 and ST/P000451/1. This work used the DiRAC Data Centric system at Durham University, operated by the Institute for Computational Cosmology on behalf of the STFC DiRAC HPC Facility (www.dirac.ac.uk). This equipment was funded by BIS National E-infrastructure capital grant ST/K00042X/1, STFC capital grant ST/H008519/1, STFC DiRAC Operations grant ST/K003267/1, and Durham University. DiRAC is part of the National E-Infrastructure.

ORCID iDs

Louis E. Strigari https://orcid.org/0000-0001-5672-6079

References

Agnello, A., & Evans, N. W. 2012, ApJL, 754, L39
Amorisco, N. C., & Evans, N. W. 2012, MNRAS, 419, 184
Battaglia, G., Helmi, A., Tolstoy, E., et al. 2008, ApJL, 681, L13
Bode, P., Ostriker, J. P., & Turok, N. 2001, ApJ, 556, 93
Breddels, M. A., Helmi, A., van den Bosch, R. C. E., van de Ven, G., & Battaglia, G. 2013, MNRAS, 433, 3173
Burkert, A. 1995, ApJL, 447, 25
Gilmore, G., Wilkinson, M. I., Wyse, R. F. G., et al. 2007, ApJ, 663, 948
Handley, W. J., Hobson, M. P., & Lasenby, A. N. 2015a, MNRAS, 450, L61
Handley, W. J., Hobson, M. P., & Lasenby, A. N. 2015b, MNRAS, 453, 4384
Laporte, C. F. P., Walker, M. G., & Peñarrubia, J. 2013, MNRAS, 433, L54
Lovell, M. R., Bose, S., Boyarsky, A., et al. 2016, MNRAS, 461, 60
Massari, D., Breddels, M. A., Helmi, A., et al. 2017, arXiv:1711.08945
Navarro, J. F., Frenk, C. S., & White, S. D. 1996, ApJ, 462, 563
Navarro, J. F., Frenk, C. S., & White, S. D. M. 1997, ApJ, 490, 493
Navarro, J. F., Ludlow, A., Springel, V., et al. 2010, MNRAS, 402, 21
Read, J. I., & Steger, P. 2017, MNRAS, 471, 4541
Richardson, T., & Fairbairn, M. 2014, MNRAS, 441, 1584
Rocha, M., Peter, A. H. G., Bullock, J. S., et al. 2013, MNRAS, 430, 81
Spergel, D. N., & Steinhardt, P. J. 2000, PhRvL, 84, 3760
Strigari, L. E., Bullock, J. S., & Kaplinghat, M. 2007, ApJL, 657, L1
Strigari, L. E., Frenk, C. S., & White, S. D. 2010, MNRAS, 408, 2364
Strigari, L. E., Frenk, C. S., & White, S. D. M. 2017, ApJ, 838, 123
Vogelsberger, M., Zavala, J., & Loeb, A. 2012, MNRAS, 423, 3740
Walker, M. G., Mateo, M., & Olszewski, E. W. 2009, AJ, 137, 3100
Walker, M. G., & Penarrubia, J. 2011, ApJ, 742, 20
White, S. D. M. 1981, MNRAS, 195, 1037
Wilkinson, M., Kleyna, J., Evans, N., & Gilmore, G. 2002, MNRAS, 330, 778